Solutions Spotlight

NEW! PlanCHECK™
Automated plan quality verification and reporting – available as part of the SunCHECK™ Platform

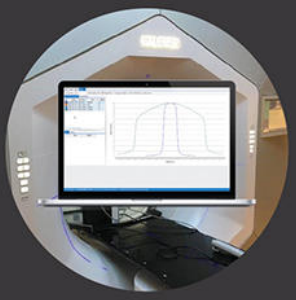

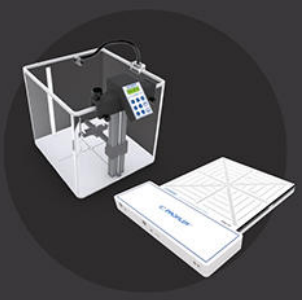

Varian Halcyon™ System Support
SNC Dosimetry™ v3.6 and 3D SCANNER™ for beam model verification and Halcyon Package for acceptance and verification

NEW! MultiPHAN™
An easy-to-use tool for comprehensive TG-142 daily alignment checks – verifying lasers to EPIDs to CBCT systems

Stereotactic Solutions
NEW SRS MapCHECK™ and StereoPHAN™ for end-to-end testing and Reference Detector for interference-free dosimetry scanning

MR-Based Radiotherapy
Custom patient and machine QA solutions, including ArcCHECK®-MR, IC PROFILER™-MR, MICRO+™ MR, and Solid Water® HE

See more. Learn more.
sunnuclear.com

SUN NUCLEAR corporation

An analytical approximation of the Bragg curve for therapeutic proton beams

Thomas Bortfeld[a)]
Deutsches Krebsforschungszentrum (DKFZ), Abteilung Medizinische Physik and Universität Heidelberg, Fakultät für Physik und Astronomie, Heidelberg, Germany

(Received 28 October 1996; accepted for publication 17 September 1997)

The knowledge of proton depth-dose curves, or ''Bragg curves,'' is a fundamental prerequisite for dose calculations in radiotherapy planning, among other applications. In various cases it is desirable to have an analytical representation of the Bragg curve, rather than using measured or numerically calculated data. This work provides an analytical approximation of the Bragg curve in closed form. The underlying model is valid for proton energies between about 10 and 200 MeV. Its main four constituents are: (i) a power-law relationship describing the range-energy dependency; (ii) a linear model for the fluence reduction due to nonelastic nuclear interactions, assuming local deposition of a fraction of the released energy; (iii) a Gaussian approximation of the range straggling distribution; and (iv) a representation of the energy spectrum of poly-energetic beams by a Gaussian with a linear ''tail.'' Based on these assumptions the Bragg curve can be described in closed form using a simple combination of Gaussians and parabolic cylinder functions. The resulting expression can be fitted to measurements within the measurement error. Very good agreement is also found with numerically calculated Bragg curves. © *1997 American Association of Physicists in Medicine.* [S0094-2405(97)00612-3]

Key words: proton beam, radiotherapy, Bragg curve, analytical approximation, parabolic cylinder function

I. INTRODUCTION

The use of high-energy proton beams in radiotherapy is becoming a topic of increasing interest as more and more proton therapy facilities are being installed. To fully exploit the potential advantages of proton or, more generally, heavy charged particle beams over conventional treatment modalities, it is necessary to perform three-dimensional treatment planning and optimization. A prerequisite for this is an algorithm for accurate and fast dose calculation. In recent years a number of such algorithms have been proposed, most of which are of the pencil beam type.[1–5]

A pencil beam algorithm composes the three-dimensional dose distribution of narrow ''pencils,'' whose weight is determined by the intensity and aperture of the beam. The pencils are in most cases described as the product of a central axis term, which is basically the depth-dose distribution (''Bragg curve'') of a broad beam,[1] and an off-axis term describing the lateral dose distribution. The off-axis term is almost always *analytically* approximated by a Gaussian with depth-dependent standard deviation.[6] The central axis term, i.e., the Bragg curve, on the other hand, is generally taken from measurements or from numerical calculations. This may be partly due to the fact that until now the problem of analytically modeling Bragg curves has been tackled in only a very few investigations. Some of the known approaches use purely mathematical curve fitting procedures,[7] and are therefore not much more generally applicable than the measured data itself.

The objective of this work is to approximate the Bragg curve with an *analytical* model that has a physical basis and that may be used to attain a fully analytical representation of the proton pencil beam. The generality of such an analytical model is particularly desirable in basic studies, e.g., in trying to determine the principle physical merit of proton therapy as compared to optimized intensity modulated photon therapy,[8] or in estimating the potential advantage of new proton treatment techniques such as ''distal edge tracking.''[9] Moreover, an analytical description of the Bragg curve may also be useful in dose calculation algorithms used for routine treatment planning, e.g., to guide inter- and extrapolation of measured data.

The paper is organized as follows: Section II describes the stepwise construction of the model for monoenergetic parallel beams, i.e., this section focuses on the machine-independent properties of the depth-dose. Section III contains a simple development of the model to roughly account for real polyenergetic beams, which are characteristic for treatment machines in clinical use. Beam divergence is not considered here because in most cases it can be taken into account by means of straightforward inverse square correction.[1] Section IV covers practical and computational aspects. Section V presents the results in form of comparisons of the model predictions with measurements and with numerical calculations performed at other institutions, and Sec. VI concludes the paper.

II. THE MODEL FOR MONOENERGETIC BEAMS

Consider an initially monoenergetic broad proton beam along the z axis, impinging on a homogeneous medium at

$z=0$. The energy fluence, Ψ, at depth z in the medium can be written in the form:

$$\Psi(z)=\Phi(z)E(z), \tag{1}$$

where $\Phi(z)$ is the particle fluence, i.e., the number of protons per cm^2, and $E(z)$ is the remaining energy at depth z. The total energy released in the medium per unit mass (the ''TERMA,'' T, Ref. 10) at depth z is then:

$$T(z)=-\frac{1}{\varrho}\frac{d\Psi}{dz}=-\frac{1}{\varrho}\left(\Phi(z)\frac{dE(z)}{dz}+\frac{d\Phi(z)}{dz}E(z)\right), \tag{2}$$

where ϱ is the mass density of the medium. The first term in the brackets represents the reduction of energy of the protons during their passage through matter. The ''lost'' energy is mainly transferred to atomic electrons. The range of these secondary electrons is negligible for our purposes. This is due to the fact that only a relatively small energy is transferred to each electron, which, in turn, is due to the small ratio of electron and proton mass (cf. Ref. 11). Therefore, the TERMA corresponding with the first term of Eq. (2) produces an absorbed dose, which is equal to the TERMA.

The second term of Eq. (2) describes the reduction of the *number* of protons. This loss of protons and the corresponding release of energy can be attributed to nonelastic nuclear interactions.[12] Here it is not so clear, where and how the released energy is absorbed. Published methods for the consideration of this effect in dose planning algorithms are largely heuristic and range from neglecting the energy[2] to assuming the local energy deposition.[5] The approach used here is somewhere between these two extremes: it is assumed that a certain fraction, γ, of the energy released in the nonelastic nuclear interactions is absorbed locally, and the rest is ignored. This approach follows the work of Berger,[13] who gives reasons why it yields reasonable results in spite of its crudeness. Some investigations show that the value of γ should be slightly higher than one half for most energies and depths.[13,4] For the sake of simplicity, in this paper $\gamma=0.6$ is used throughout.

The total absorbed dose, $\hat{D}(z)$, is consequently given by

$$\hat{D}(z)=-\frac{1}{\varrho}\left(\Phi(z)\frac{dE(z)}{dz}+\gamma\frac{d\Phi(z)}{dz}E(z)\right). \tag{3}$$

In order to determine this depth-dose curve, we only need to know the functional relations $E(z)$ and $\Phi(z)$. These are obtained from the known range-energy relationship and the probability of nonelastic nuclear interactions, respectively.

A. Range-energy relationship

The relationship between the initial energy $E(z=0)=E_0$ and the range $z=R_0$ in the medium is approximately given by

$$R_0=\alpha E_0^p. \tag{4}$$

With $p=1.5$, this relationship is known as Geiger's rule,[14] which is valid for protons with energies up to about 10 MeV. For energies between 10 and 250 MeV the exponent p increases to $p\approx1.8$.[14,15] The factor α is approximately proportional to the square root of the effective atomic mass of the absorbing medium, $\sqrt{A_{\text{eff}}}$ (''Bragg–Kleeman rule''[14]). It is also inversely proportional to the mass density of the medium.

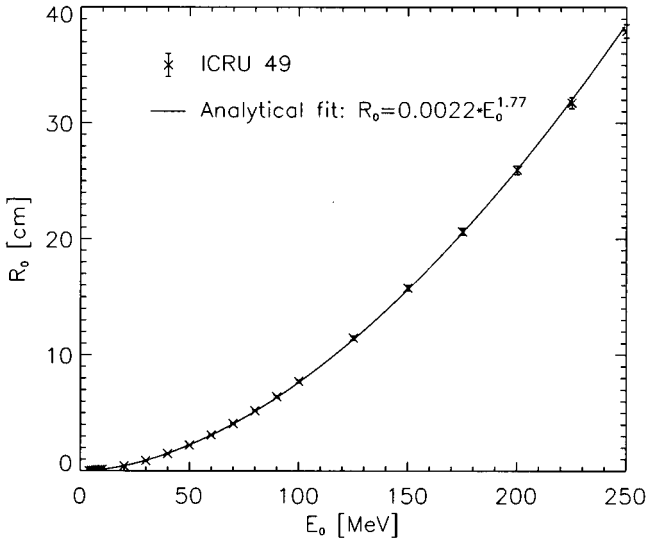

FIG. 1. Range-energy relationship according to ICRU 49 (Ref. 16) and analytical fit with Eq. (4). The error bars represent a relative error of the ICRU data of $\pm1.5\%$.

In the present work a new fit of Eq. (4) to the range-energy table published by ICRU[16] was performed. The fitting process was driven by the constraint that for the most relevant energies, i.e., $0\leqslant E_0\leqslant200$ MeV, the maximum deviation between approximation (4) and the ICRU range should be less than ±1.5 mm. Using the inverse of Eq. (4) for $R_0\leqslant0.5$ cm, and assuming E_0 to be given in units of MeV and R_0 in cm, the best fit of $E_0(R_0)$ to the ICRU data gave $p\approx1.77$ and $\alpha\approx2.2\times10^{-3}$ for protons in water (cf. Fig. 1).

Because of the statistical nature of the interaction of radiation with matter, actual ranges are distributed about a mean range with an approximately Gaussian distribution. The above formula holds for the mean range. The ''range straggling'' effect will be considered later. For the moment we will assume that all protons of the same initial energy have exactly the same range.

The beam deposits energy along its path between $z=0$ and $z=R_0$ in the medium. The remaining energy $E(z)$ at an arbitrary depth $z\leqslant R_0$ must just suffice to travel the distance R_0-z. Thus, according to the range-energy relationship: $R_0-z=\alpha E^p(z)$, or

$$E(z)=\frac{1}{\alpha^{1/p}}(R_0-z)^{1/p}. \tag{5}$$

This is the expression for the residual energy as a function of the depth, which we were looking for. The linear stopping power is now given by

$$S(z)=-\frac{dE}{dz}=\frac{1}{p\alpha^{1/p}}(R_0-z)^{1/p-1}. \tag{6}$$

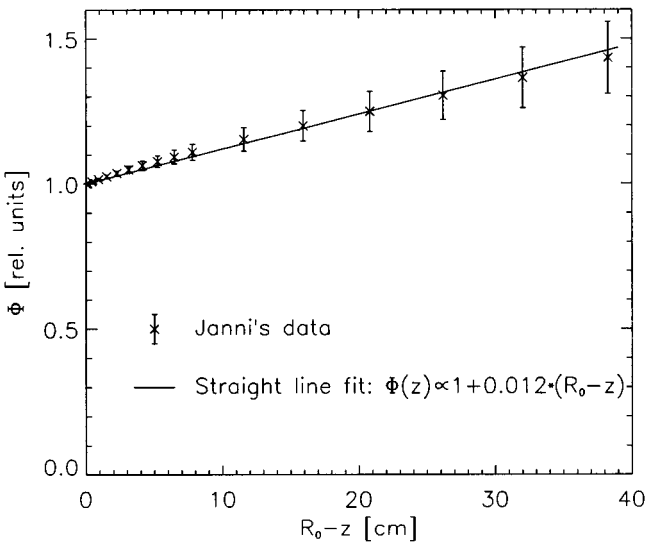

FIG. 2. Fluence reduction according to Janni's data (Ref. 12) using Eq. (7), and its straight line fit. The error bars are also based on Janni's data, with consideration of error propagation.

B. Fluence reduction

For energies above about 20 MeV there is nonnegligible probability that protons may be lost from the beam due to nuclear interactions. The probability, P, for such nonelastic nuclear interactions as a function of the residual range, $R_0 - z$, has been tabulated by Janni.[12] Lee *et al.*[2] have derived the proportionality

$$\Phi(z) \propto \frac{1}{1-P(R_0-z)}. \tag{7}$$

These data are plotted in Fig. 2. The reduction of the fluence from $z=0$ to $z=R_0$ can be roughly approximated by a straight line:[2]

$$\Phi(z) \propto 1+\beta(R_0-z), \tag{8}$$

which is also plotted in Fig. 2. [A slightly better approximation results from the use of another power-law relationship, particularly: $\Phi(z) \propto 1+0.018(R_0-z)^{0.87}$. Nevertheless, the straight line fit will be used due to its simplicity.] The slope parameter, β, was determined to be $\beta \approx 0.012\ \mathrm{cm}^{-1}$. For practical reasons it is more useful to normalize the fluence to the primary fluence, Φ_0, which yields

$$\Phi(z) = \Phi_0 \frac{1+\beta(R_0-z)}{1+\beta R_0}. \tag{9}$$

The fluence reduction at depth z is then

$$-\frac{d\Phi}{dz} = \Phi_0 \frac{\beta}{1+\beta R_0}. \tag{10}$$

C. Depth dose without range straggling

The depth-dose distribution can now be calculated simply by inserting Eqs. (5), (6), (9), (10), into Eq. (3). This yields

$$\hat{D}(z) = \begin{cases} \Phi_0 \dfrac{(R_0-z)^{1/p-1} + (\beta+\gamma\beta p)(R_0-z)^{1/p}}{\varrho p \alpha^{1/p}(1+\beta R_0)} \\ \quad \text{for } z<R_0 \\ 0 \quad \text{for } z>R_0 \end{cases} \tag{11}$$

which is of the form,

$$\hat{D}(z) = \hat{D}_1(z) + \hat{D}_2(z) = a_1(R_0-z)^{1/p-1} + a_2(R_0-z)^{1/p}. \tag{11a}$$

The fist term, $\hat{D}_1(z)$, is the dose contribution from those protons that have no nuclear interactions. It is proportional to the (nonnuclear) stopping power and exhibits to some degree the form of a Bragg curve, as it increases monotonically from $z=0$ to $z=R_0$ and has a peak at R_0. However, due to the neglect of range straggling, the peak is unrealistically sharp, and there is a singularity at $z=R_0$. The second term, $\hat{D}_2(z)$, represents the dose delivered by the relatively small fraction of protons that have nuclear interactions. It *decreases* monotonically and is zero at $z=R_0$ (cf. Fig. 3). Note that $\hat{D}_2(z)$ comprises the dose resulting not only from nuclear but also from nonnuclear interactions that take place before the nuclear collision.

Expression (11) gives $\hat{D}$ in units of MeV/g, if ϱ is given in g/cm^3. To obtain $\hat{D}$ in Gy, one needs to multiply with the factor $10^9 e/C = 1.602 \times 10^{-10}$, where e is the elementary charge.

D. Depth-dose with range straggling

Let us first consider only those protons that have no nuclear interactions, referring to $\hat{D}_1(z)$ of Eq. (11). For statistical reasons we should expect that the distribution of the range of individual protons that have lost all their energy E_0 in the matter is Gaussian.[11] This is in fact a good approximation, although the real distribution is slightly asymmetric because of multiple *elastic* scattering, which can make the (projected) range smaller but never larger.[17]

Similarly, the distribution of the (projected) depth at which the protons have lost the part E_0-E of their energy is approximately a Gaussian distribution about the mean depth $\bar{z}(E,E_0)$ with standard deviation $\sigma_z(\bar{z})$. Thus there is an uncertainty in the depth at which the protons have a residual energy of E, which can be considered as depth straggling. On the other hand, the residual energy E determines *exactly* the stopping power, hence $\hat{D}_1$. Therefore the dose delivered right after the protons have lost the energy E_0-E may be written as $\hat{D}_1(\bar{z}(E,E_0))$. The dose $D_1(z)$ at the *actual* depth z is then obtained by folding the Gaussian depth straggling into $\hat{D}_1$ by means of

$$D_1(z) = \langle \hat{D}_1 \rangle(z) = \int_0^{R_0} \hat{D}_1(\bar{z}) \frac{e^{-(z-\bar{z})^2/2\sigma_z^2(\bar{z})}}{\sqrt{2\pi}\sigma_z(\bar{z})}\, d\bar{z}. \tag{12}$$

The calculation of $D_2(z)$, i.e., the consideration of straggling for the fraction of protons that have nuclear interactions, is less straightforward but also less critical, because these protons contribute a smaller and smoother amount to

the total dose. At this point we will assume that straggling can be folded into $\hat{D}_2$ in exactly the same way as above, i.e., that we can simply replace $\hat{D}_1$ by $\hat{D}_2$ in Eq. (12) to obtain $D_2(z)$.

Since the protons accumulate depth straggling along their path (cf. Appendix B), $\sigma_z(\bar{z})$ is strongly depth dependent, starting with $\sigma_z(0)=0$ and reaching a maximum of σ: $=\sigma_z(R_0)$. Nevertheless, it was found that the integral in Eq. (12) can be approximated with very high accuracy by assuming a constant value of $\sigma_z(\bar{z})\equiv\sigma$. This can be understood because at those depths where $\sigma_z(\bar{z})$ is significantly smaller than σ, both $\hat{D}_1$ and $\hat{D}_2$ are smooth, such that the effect of folding in a Gaussian is negligible (cf. Fig. 3).

Consequently, we can write $D(z)=D_1(z)+D_2(z)$ as the convolution integral

$$D(z)=\langle\hat{D}\rangle(z)=\frac{1}{\sqrt{2\pi}\sigma}\int_{-\infty}^{R_0}\hat{D}(\bar{z})e^{-(z-\bar{z})^2/2\sigma^2}d\bar{z}. \quad (13)$$

In Appendix B it is shown that the convolution of the terms $(R_0-z)^{\nu-1}$ of Eq. (11) with the Gaussian yields

$$(R_0-z)^{\nu-1}\mapsto\frac{1}{\sqrt{2\pi}\sigma}\,e^{-(R_0-z)^2/4\sigma^2}\sigma^{\nu}\Gamma(\nu)\times\mathscr{D}_{-\nu}\left(-\frac{R_0-z}{\sigma}\right), \quad (14)$$

where $\Gamma(x)$ is the gamma function and $\mathscr{D}_y(x)$ is the parabolic cylinder function.[18,19] Inserting this result into Eq. (11) yields

$$D(z)=\Phi_0\,\frac{e^{-\zeta^2/4}\sigma^{1/p}\Gamma(1/p)}{\sqrt{2\pi}\varrho p\alpha^{1/p}(1+\beta R_0)}\times\left[\frac{1}{\sigma}\,\mathscr{D}_{-1/p}(-\zeta)+\left(\frac{\beta}{p}+\gamma\beta\right)\mathscr{D}_{-1/p-1}(-\zeta)\right] \quad (15)$$

with

$$\zeta=\frac{R_0-z}{\sigma}. \quad (16)$$

The value of $\sigma=\sigma_{\text{mono}}$ for an initially mono-energetic beam depends on R_0 (or E_0). The functional relation can be approximated by

$$\sigma^2\approx\alpha'\,\frac{p^3\alpha^{2/p}}{3p-2}\,R_0^{3-2/p}, \quad (17)$$

where α' is a factor that, as α, depends on the stopping matter (Appendix B). For water we find $\alpha'=0.087$ MeV^2/cm, and consequently

$$\sigma\approx 0.012R_0^{0.935}, \quad (18)$$

where R_0 and σ are in cm (cf. Ref. 20). This means that σ is approximately proportional to R_0 with a value roughly 1% of R_0.

As an example we will consider a mono-energetic 150 MeV proton beam in water. From the range-energy relationship (4) we find $R_0=15.64$ cm, and with Eq. (18) we obtain $\sigma=0.16$ cm. The resulting Bragg curves with and without consideration of straggling as calculated with Eq. (15) and (11), respectively, are shown in Fig. 3.

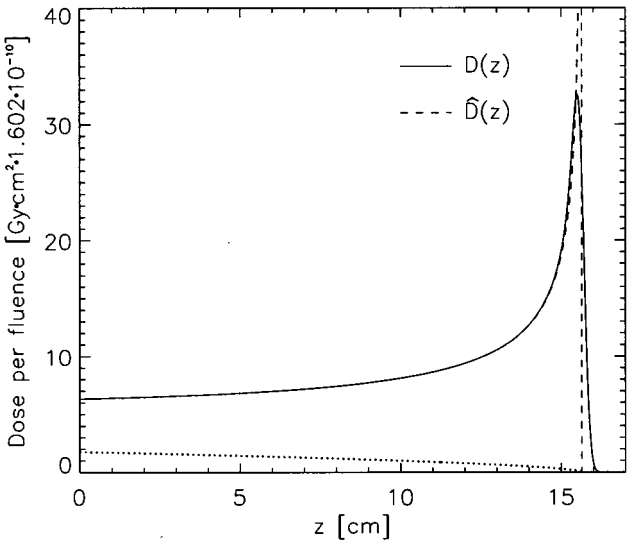

FIG. 3. Bragg curves with and without consideration of straggling for 150 MeV protons in water. The dotted line at the bottom is the dose contribution from the fraction of protons that have nuclear interactions, i.e., $D_2(z)$ or $\hat{D}_2(z)$ (these are indistinguishable within the resolution of the figure).

III. CONSIDERATION OF THE ENERGY SPECTRUM

So far it has been assumed that the proton beam is initially mono-energetic. Unfortunately, this assumption does not correspond with reality. Real beams have an initial spectral energy distribution, which depends on the individual characteristics of the accelerator, the beam guide, and the collimation system. The energy spectrum $\Phi_E(E)\Delta E$, which is the number of protons per cm^2 with energies between E and $E+\Delta E$, can be quite different from the ideal δ-shape. An obvious way to consider the energy spectrum is to perform a weighted superposition of mono-energetic Bragg curves with weights Φ_E. In general, there is no analytical solution to this problem, so that numerical methods have to be used. In this work we will use an approximation, which allows for an analytical solution of the form of Eq. (15).

Typical energy spectra consist of two parts: A peak, which can be approximated by a Gaussian energy spectrum around $E=E_0$, and a relatively small ''tail'' extending toward low energies. Let $\sigma_{E,0}$ be the standard deviation of the Gaussian. Since $\sigma_{E,0}$ is generally small ($\sigma_{E,0}\ll E$), the range-energy relationship of Eq. (4) can be linearized around $E=E_0$. Hence, the Gaussian energy spectrum translates into a Gaussian range spectrum, whose variance adds to the σ_{mono}^2 of the mono-energetic beam:

$$\sigma^2=\sigma_{\text{mono}}^2+\sigma_{E,0}^2\left(\frac{dR_0}{dE_0}\right)^2=\sigma_{\text{mono}}^2+\sigma_{E,0}^2\alpha^2p^2E_0^{2p-2}. \quad (19)$$

TABLE I. Summary of constants and parameters used in the theoretical model. The values are for protons in water. The last two parameters are machine specific. The value of σ can be calculated from σ_{mono} and $\sigma_{E,0}$ using Eq. (19).

	Description	Value	Unit
p	Exponent of range-energy relation	1.77	1
α	Proportionality factor	0.0022	cm MeV^{-p}
R_0	Range	αE_0^p	cm
β	Slope parameter of fluence reduction relation	0.012	cm^{-1}
γ	Fraction of locally absorbed energy released in nonelastic nuclear interactions	0.6	1
σ_{mono}	Width of Gaussian range straggling	$0.012R_0^{0.935}$	cm
$\sigma_{E,0}$	Width of Gaussian energy spectrum	$\approx 0.01E_0$	MeV
ϵ	Fraction of primary fluence contributing to the ''tail'' of the energy spectrum	$\approx 0.0-0.2$	1

Consequently, the Gaussian energy spectrum can be considered simply by increasing the σ in Eq. (15) as compared to its value from Eq. (17). (Note that in the previous section we basically dealt with Gaussian *depth* spectra, while here we have to account for a Gaussian *range* spectrum. However, since the depth-dose depends primarily on the distance between range and depth, this conceptual difference has no practical significance.)

The consideration of the tail of the energy spectrum is somewhat more difficult because it may depend on many different factors, and its exact shape is not generally known. Fortunately, we can utilize the fact that the total fluence corresponding with the tail is only a relatively small fraction, ϵ, of the fluence Φ_0 in the peak. For this reason, we can use rather coarse models to approximate the spectrum of the tail. A very simple model that agrees at least with the expectation that $\Phi_E(E)$ should be negligible at $E=0$ and have a positive slope for small E is a linear ramp: $\Phi_E(E) \propto E$ for $0 \leqslant E \leqslant E_0$. Normalizing the integral of $\Phi_E(E)$ to $\epsilon\Phi_0$ yields

$$\Phi_E(E) = \epsilon\Phi_0 \frac{2E}{E_0^2}. \tag{20}$$

To avoid a discontinuity of the energy spectrum at $E=E_0$, the sharp edge of the ramp should be ''smeared.'' This will be done implicitly by means of the incorporation of straggling later on. It should be noted that the average tail-to-peak ratio of the energy spectrum is $\sqrt{2\pi}\sigma_{E,0}\epsilon/E_0$, which is in the order of only 2%-3% of ϵ.

To calculate the depth-dose distribution resulting from the linear energy spectrum, it is necessary to translate $\Phi_E(E)$ into a range spectrum $\Phi_R(R)$, where $\Phi_R(R)\Delta R$ is the fluence of protons with ranges between R and $R+\Delta R$. This is accomplished by means of the relation $\Phi_R(R) = \Phi_E(E(R))dE/dR$. Using the range-energy relationship of Eq. (4) gives

$$\Phi_R(R) = \epsilon\Phi_0 \frac{2R^{2/p-1}}{E_0^2 p \alpha^{2/p}}. \tag{21}$$

This means that the range spectrum resulting from the linear energy spectrum is approximately constant ($2/p-1 \ll 1$). In fact, with the approximation $p \approx 2$ we obtain:

$$\Phi_R(R) \approx \text{const.} = \epsilon\Phi_0 \frac{1}{R_0}. \tag{22}$$

The range spectrum must be convolved with the individual depth-dose distribution as a function of the range to obtain the total depth-dose distribution, D_{tail}, resulting from the tail of the energy spectrum. Again, we can make simplifications, which can be justified due to the relatively small value of ϵ. First, we will go back to the case where range straggling was ignored. Here the dose delivered by protons that have nuclear interactions will be disregarded, i.e., it will be assumed that $\hat{D}(z) = \hat{D}_1(z)$ [cf. Eqs. (11), (11a)]. Now we can write $\hat{D}_1$ as a function of z and R (instead of R_0) and perform the convolution as follows:

$$\hat{D}_{\text{tail}}(z) \approx \frac{1}{\Phi_0} \int_z^{R_0} \Phi_R(R)\hat{D}_1(z,R)dR \tag{23}$$

$$\approx \frac{\epsilon\Phi_0}{R_0 \varrho p \alpha^{1/p}(1+\beta R_0)} \int_z^{R_0} (R-z)^{1/p-1} dR \tag{24}$$

$$= \frac{\epsilon\Phi_0}{R_0 \varrho \alpha^{1/p}(1+\beta R_0)} (R_0-z)^{1/p}. \tag{25}$$

Note that this expression is of the same form as the second term, $\hat{D}_2(z)$, of Eq. (11). Straggling can now be considered in the same way as in the previous section, which results in the final expression $D_{\text{tail}}(z)$. Adding this expression to the $D(z)$ of Eq. (15) gives

$$D(z) = \Phi_0 \frac{e^{-\zeta^2/4}\sigma^{1/p}\Gamma(1/p)}{\sqrt{2\pi}\varrho p \alpha^{1/p}(1+\beta R_0)} \left[\frac{1}{\sigma} \mathscr{D}_{-1/p}(-\zeta) + \left(\frac{\beta}{p} + \gamma\beta + \frac{\epsilon}{R_0} \right) \mathscr{D}_{-1/p-1}(-\zeta) \right]. \tag{26}$$

IV. COMPUTATIONAL METHODS

At first glance Eq. (26) looks rather complicated. However, its length is mainly due to the many constants involved. Table I summarizes the constants and parameters for convenience.

The ''heart'' of Eq. (26) is the parabolic cylinder function $\mathscr{D}_y(x)$. This function is tabulated.[18] Public domain computer programs for the calculation of $\mathscr{D}_y(x)$ are available. For $\zeta > 20$ numerical problems may occur because $\mathscr{D}(\zeta)$ becomes very large. However, for $\zeta > 10$ (i.e., $z < R_0 - 10\sigma$), $D(z)$ agrees with $\hat{D}(z)$ to within 0.5% (cf. Fig. 3). Furthermore, for $\zeta < -5$ (i.e., $z > R_0 + 5\sigma$), $D(z)$ is negligible. Therefore, we can approximate $D(z)$ by

$$D(z) \approx \begin{cases} \hat{D}(z) & \text{for} \quad z < R_0 - 10\sigma \\ D(z) & \text{for} \quad R_0 - 10\sigma \leqslant z \leqslant R_0 + 5\sigma \\ 0 & \text{otherwise.} \end{cases} \tag{27}$$

Alternatively, we can directly compute $\exp(-x^2/4)\mathscr{D}_y(x)$, which is well-behaved for arbitrary (real) x values, and y values relevant to this study. A FORTRAN computer program for this calculation is available from the author on request.

The gamma function, which is required in Eq. (26), is tabulated and be computed within many commercially available mathematical computer programs. For the p value from Table I we find: $\Gamma(1/p) = 1.575$. The depth-dose distribution in water is therefore determined by

$$\hat{D}_{H_2O}(z) = \frac{\Phi_0}{1 + 0.012 R_0} [17.93 (R_0 - z)^{-0.435} + (0.444 + 31.7\epsilon/R_0)(R_0 - z)^{0.565}] \tag{28}$$

and

$$D_{H_2O}(z) = \Phi_0 \frac{e^{-(R_0 - z)^2/4\sigma^2} \sigma^{0.565}}{1 + 0.012 R_0} \times \left[11.26 \sigma^{-1} \mathscr{D}_{-0.565}\left(-\frac{R_0 - z}{\sigma} \right) + (0.157 + 11.26\epsilon/R_0) \mathscr{D}_{-1.565}\left(-\frac{R_0 - z}{\sigma} \right) \right]. \tag{29}$$

V. COMPARISONS WITH MEASURED AND NUMERICALLY CALCULATED DATA

To investigate the quality of the analytical approximation (26) or (29), comparisons were made with measured and numerically calculated depth-dose data. Since the energy spectra of the beams were not generally known, the parameters σ, ϵ, and R_0 were varied to achieve an optimum fit to the measured data. (It should be noted that measured depth-dose curves depend to some degree on the dosimeter.[21] Careful dosimetry is essential if one wishes to determine the parameters σ and ϵ that are characteristic of the beam, and not of the technique of measurement.) The value of R_0 could also be determined from the range-energy relationship (4) using the known nominal (extraction) energy of the accelerator. However, for various reasons the nominal energy did not agree very well with E_0 of the beam. Therefore it was chosen to use R_0 as a fit parameter. In most cases the Bragg curves were normalized to a maximum of 1.0 because no absolute dose values were available. The fit was performed by means of trial and error. The development of an automatic fit procedure should be relatively easy. However, the pressure to develop such an algorithm was not very high because in general very few (about five) iterations sufficed to achieve good results. For the comparisons with the numerical data all parameters were directly taken from Table I, without any fitting.

TABLE II. Parameters for the fit of Eq. (29) to measured data published in the literature.

Source	R_0 [cm]	σ [cm]	ϵ [%]	Max. Deviation [%]	Max. Deviation [cm]
Larsson (Ref. 22)	23.4	0.29	2	−2.3	+0.14
Koehler *et al.* (Ref. 23)	15.8	0.27	5	−2.5	−0.10

Incidentally, a general and elegant check of the depth-dose distribution is based on the rule that R_0 equals the depth z_{80} at which the dose has dropped to 80% of its maximum value beyond the Bragg peak.[13] The analytical model of this work confirms this rule. In fact, if nuclear interactions and the effect of the energy tail are disregarded near the Bragg peak, the relation $z_{80} = R_0$ can be derived from Eq. (26). Under these assumptions the relation is strictly valid for all R_0, σ, and α.

A. Comparisons with measured data

As a first step, the model was compared with measured data published in the literature. In particular, the data published in Fig. 5 of Larsson[22] for the synchrocyclotron at Uppsala and in Fig. 2 of Koehler *et al.*[23] for the Harvard cyclotron laboratory (HCL) were considered. The corresponding values of the parameters and the maximum deviations are presented in Table II. The deviations are given in % for the plateau region and in cm for the peak region. As can be seen from this table, the agreement is very good. Deviations are in the order of magnitude of reading the data off the figures.

Second, the analytical model was compared with measured data, which was kindly provided by several proton centers. As a first example measured data from the radiosurgery beam line of the HCL was considered. The measurements were performed with a Markus parallel plate chamber in a water tank. The beam was collimated to 4.8 cm diameter, representing a broad beam. The nominal energy was 158.6 MeV, but there was some energy loss in the scattering systems and in the tank wall, resulting in a range, R_0, of only 13.5 cm. The beam divergence effect was removed from the measurements by means of inverse square division. Figure 4 shows the data and their analytical fit. A relatively high value of ϵ (20%) had to be used to achieve a good fit in this example. However, there is a considerable amount of uncertainty in this value because the effect resulting from the

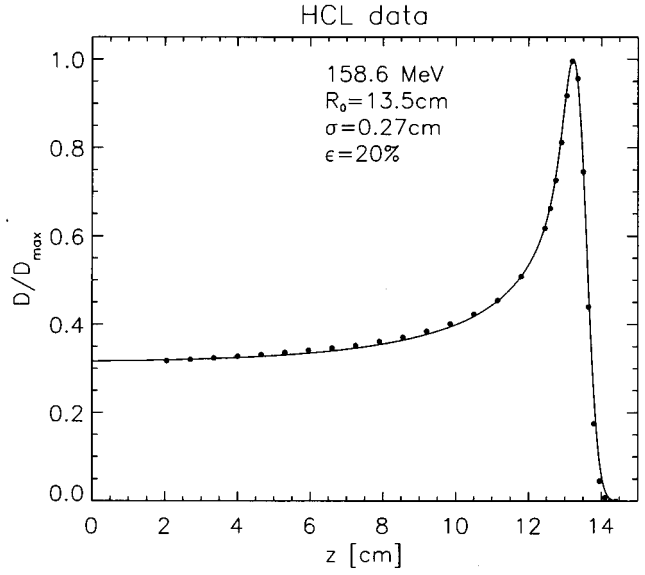

FIG. 4. Depth-dose measurements in water (big dots) for the HCL beam. The solid line represents the analytical fit using $D_{H_2O}(z)$ of Eq. (29).

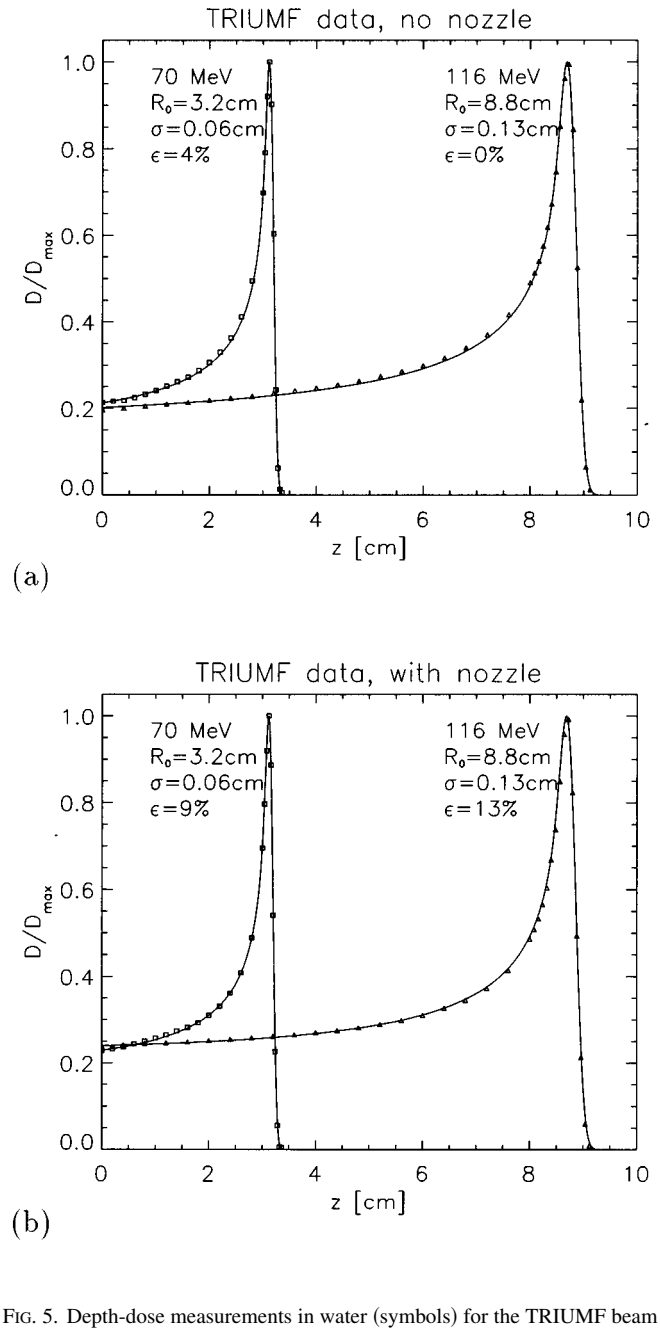

FIG. 5. Depth-dose measurements in water (symbols) for the TRIUMF beam with (a) and without (b) nozzle in the beam path. The estimated measurement error is roughly given by the size of the symbols. The solid lines represent the analytical fit using $D_{H_2O}(z)$ of Eq. (29).

tail of the energy spectrum and the divergence effect cannot be fully separated (both result in an increased entrance dose), and because the degree of divergence was not exactly known.

As a second example a dataset from TRIUMF (TRI University Meson Facility), Vancouver, Canada was considered. The dataset consisted of measurements with and without the proton nozzle in the beam path, and for two nominal energies, 70 MeV and 116 MeV, each. No collimators were inserted, such that the data represents a broad beam. The measurements were carefully performed with an optical diode (type BPW34) in a water phantom.[5,24] Again, the beam divergence effect was removed from the measurements by means of inverse square division before comparison with the analytical model. Figure 5 shows the very good fit obtained. Deviations are within the measurement error, which is approximately given by the size of the symbols. Obviously, the nozzle causes some additional low-energy contamination of the beam, thus requiring a higher value of ϵ for the fit.

B. Comparisons with numerically calculated data

As a further test of the model, comparisons were made with numerically calculated Bragg curves, which were taken from dose calculation algorithms developed at TRIUMF in collaboration with DKFZ,[5] and at PSI (Paul Scherrer Institute), Villigen, Switzerland.[4] Both algorithms were verified through measurements and Monte Carlo calculations. In this case no normalization had to be done because the numerical results were given in absolute terms.

Figure 6(a) shows the comparisons for a mono-energetic 175 MeV Bragg curve from the TRIUMF algorithm (dashes). The solid line results from applying Eq. (29) with all parameters calculated using the methods presented in this work. Particularly, σ was determined to be 0.2 cm from Eq. (18) alone, as $\sigma_{E,0}$ should be zero for a mono-energetic beam. For the same reason, ϵ was set to zero. The comparison shows that the analytical model predicts a 5% higher peak dose than the TRIUMF algorithm, while the entrance dose is somewhat smaller. The reasons for this discrepacy can be manifold and are not yet completely understood. However, it should be noted that by slightly increasing the value of σ to 0.23 cm, and setting $\epsilon = 6\%$, an excellent fit can be achieved. This could not be demonstrated in Fig. 6(a) because the curve was indistinguishable from the dashed TRIUMF curve.

The PSI examples shown in Fig. 6(b) (dashes) are calcu-

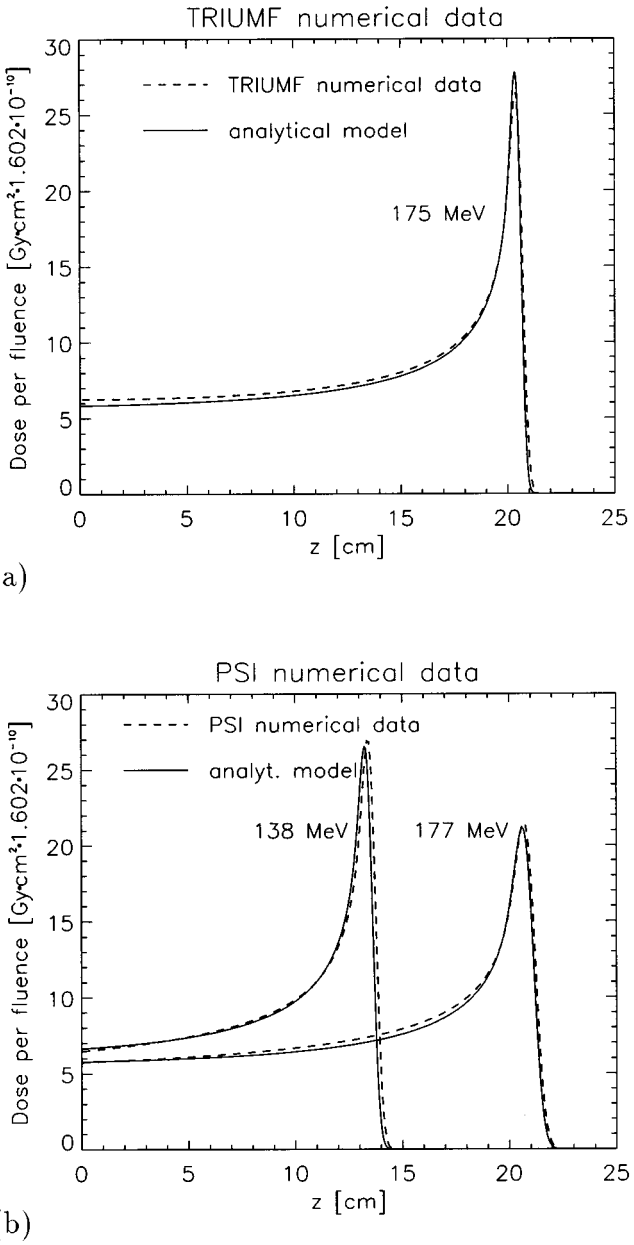

FIG. 6. Comparison of numerically calculated Bragg curves (----) with the analytical model (—) of this work, Eq. (29), using the parameters of Table I without fitting. (a): data from TRIUMF (Ref. 5); (b): data from PSI (Ref. 4).

lated Bragg curves for 138 MeV and 177 MeV beams with a Gaussian energy spectrum. From the known values of the momentum band of the beam, the values of $\sigma_{E,0}$ were determined to be 1.32 MeV and 1.52 MeV, respectively. All other parameters were taken from Table I; ϵ was set to zero. The resulting analytical curves (solid lines) show good agreement with the PSI curves. In the 138 MeV data there is an apparent shift corresponding with an error in R_0 of 1 mm. Other parameters such as the entrance dose and the width and height of the Bragg peak agree very well. In the 177 MeV example there is a minor deviation at medium depths. The most likely explanation for this is that the PSI algorithm includes a nonlocal model for the consideration of the dose produced by nonelastic nuclear interactions, which causes an increased dose at medium depths.[4]

VI. DISCUSSION AND CONCLUSIONS

It has been shown that the depth-dose curve of a broad proton beam perpendicularly incidenting on a homogeneous medium can be represented analytically through terms given by the product of a Gaussian and a parabolic cylinder function. In a way this can be seen as a ''natural'' representation of the proton Bragg curve, just like the depth-dose curve of a proton beam can be described by means of exponentials. This analytical expression for the Bragg curve is derived from several phenomenological approximations of the interaction principles of protons with matter, and it is based on a coarse model of the primary energy spectrum of typical beams. The validity of these approximations is proved by the fact that the model can easily be fitted to measured data within the error of measurement. Very good agreement has also been found without parameter fitting between the model predictions and numerical depth-dose data calculated at other institutions. The model is valid for clinically relevant energies up to about 200 MeV. In most cases that have been studied a systematic deviation at depths around 3/4 of the maximum range has been found, where the model predictions are consistently slightly too low. This might be attributed to the coarse approximation of the energy spectrum. However, a more likely explanation is the oversimplified model for the dose deposition resulting from nuclear interactions. Here some further development might be worthwhile, though the deviations are very small, with less than 3% relative deviation.

Potential applications of the closed form representation of the Bragg curve are primarily seen in theoretical studies regarding radiotherapy planning and optimization. Furthermore, the model may also be useful in clinical treatment planning programs. One point of practical concern is the calculation speed. ''Brute force'' calculations of the product of the Gaussian with the parabolic cylinder function are relatively slow. However, there is some potential for improvements. For example, it seems possible to resolve this product into cubic splines, which allows for a very rapid calculation (E. de Kock, NAC, private communication).

It is evident that the knowledge of the Bragg curve alone is not sufficient for any practical application. However, methods for the consideration of other relevant effects, of which the most important ones are the lateral widening of the beam at depth due to multiple coulomb scattering, and the influence of inhomogeneities, are well known. The lateral dose fall-off can be modeled simply and accurately using Gaussian kernels.[6] The simplest form of an inhomogeneity correction method, which still is sufficiently accurate in most cases, is a pathlength scaling approach.

ACKNOWLEDGMENTS

I would like to thank Dr. K.-U. Gardey, Dr. A. Lomax, Dr. M. Goitein, Dr. K. P. Gall, Dr. C. Dykstra, and Dr. E. de

Kock for helping me in various ways, particularly by providing their measured and numerically calculated Bragg curves for this study, and through fruitful discussions. Special thanks go to Dr. U. Oelfke for very detailed and helpful hints on the manuscript. I am grateful to an unknown referee for very interesting comments, and for the reference to the $z_{80}=R_0$ rule.

APPENDIX A: MATHEMATICAL CONSIDERATION OF RANGE STRAGGLING

We wish to convolve terms of the form $(R_0-z)^{\nu-1}$ from the numerator of Eq. (11) with the Gaussian depth straggling distribution, i.e., we calculate

$$F(z,R_0)=\frac{1}{\sqrt{2\pi}\sigma}\int_{-\infty}^{R_0}(R_0-\bar{z})^{\nu-1}e^{-(z-\bar{z})^2/2\sigma^2}d\bar{z}. \quad \text{(A1)}$$

Setting

$$u:=R_0-\bar{z}, \quad v:=R_0-z \quad \text{(A2)}$$

yields

$$F(v)=\frac{1}{\sqrt{2\pi}\sigma}\int_0^{\infty}u^{\nu-1}e^{-(u-v)^2/2\sigma^2}du \quad \text{(A3)}$$

$$=\frac{1}{\sqrt{2\pi}\sigma}e^{-v^2/2\sigma^2}\int_0^{\infty}u^{\nu-1}e^{-(u^2-2uv)/2\sigma^2}du. \quad \text{(A4)}$$

This integral can be solved in closed form (e.g., Ref. 19, p. 337). The result is

$$F(v)=\frac{1}{\sqrt{2\pi}\sigma}e^{-v^2/2\sigma^2}\left(\frac{1}{\sigma^2}\right)^{-\nu/2}\Gamma(\nu)e^{v^2/4\sigma^2}\mathscr{D}_{-\nu}\left(-\frac{v}{\sigma}\right) \quad \text{(A5)}$$

$$=\frac{1}{\sqrt{2\pi}\sigma}e^{v^2/4\sigma^2}\sigma^{\nu}\Gamma(\nu)\mathscr{D}_{-\nu}\left(-\frac{v}{\sigma}\right), \quad \text{(A6)}$$

where $\Gamma(x)$ is the gamma function and $\mathscr{D}_y(x)$ is the parabolic cylinder function.[18,19]

APPENDIX B: DETERMINATION OF THE RANGE STRAGGLING WIDTH

The mean square fluctuation in the range, σ^2, for a given initial energy can be determined from the mean square fluctuation in the residual energy, σ_E^2, at given depths using:[11]

$$\sigma^2=\int_0^{R_0}\frac{d}{dz}(\sigma_E^2)\left(\frac{dE}{dz}\right)^{-2}dz. \quad \text{(B1)}$$

For energies above about 10 MeV the term $d/dz(\sigma_E^2)$ can be approximated using Bohr's classical formula (cf. Refs. 11, 25):

$$\frac{d}{dz}(\sigma_E^2)\approx\frac{1}{4\pi\epsilon_0^2}e^4NZ=:\alpha'. \quad \text{(B2)}$$

Here e is the electron charge, and NZ is the electron density of the stopping matter. For water we obtain: $\alpha'\approx 0.087\ \text{MeV}^2/\text{cm}$.

Inserting the stopping power from Eq. (6) into Eq. (36) we can now calculate σ^2:

$$\sigma^2=\alpha'\int_0^{R_0}\left(\frac{1}{p\alpha^{1/p}}(R_0-z)^{1/p-1}\right)^{-2}dz \quad \text{(B3)}$$

$$=\alpha' p^2\alpha^{2/p}\int_0^{R_0}(R_0-z)^{2-2/p}dz \quad \text{(B4)}$$

$$=\alpha'\frac{p^2\alpha^{2/p}}{3-2/p}R_0^{3-2/p}. \quad \text{(B5)}$$

[a]Electronic-mail: t.bortfeld@dkfz-heidelberg.de

[1]L. Hong, M. Goitein, M. Bucciolini, R. Comiskey, B. Gottschalk, S. Rosenthal, C. Serago, and M. Urie, ''A pencil beam algorithm for proton dose calculations,'' Phys. Med. Biol. **41**, 1305–1330 (1996).
[2]M. Lee, A. E. Nahum, and S. Webb, ''An empirical method to build up a model of proton dose distribution for a radiotherapy treatment planning package,'' Phys. Med. Biol. **38**, 989–998 (1993).
[3]P. L. Petti, ''Differential pencil-beam dose calculation for charged particles,'' Med. Phys. **19**, 137–149 (1992).
[4]S. Scheib, ''Spot-Scanning mit Protonen: Experimentelle Resultate und Therapieplanung,'' Ph.D. thesis, ETH Zürich, 1993.
[5]K.-U. Gardey, ''A Pencil Beam Model for Proton Therapy—Treatment Planning and Experimental Results,'' Ph.D. thesis, Universität Heidelberg, 1996.
[6]B. Gottschalk, A. M. Koehler, R. J. Schneider, J. M. Sisterson, and M. S. Wagner, ''Multiple Coulomb scattering of 160 MeV protons,'' Nucl. Instrum. Methods Phys. Res. B **74**, 467–490 (1993).
[7]C. V. Levin, R. Gonin, and S. Wynchank, ''Computed limitations of spot scanning for therapeutic proton beams,'' Int. J. Biomed. Comput. **23**, 33–41 (1988).
[8]A. Brahme *et al.*, ''Optimization of the three-dimensional dose delivery and tomotherapy,'' Int. J. Imaging Syst. Technol. **6**, 1–128 (1995).
[9]J. O. Deasy, D. M. Shepard, and T. R. Mackie, ''Distal edge tracking: A proposed delivery method for conformal proton therapy using intensity modulation,'' *XIIth International Conference on the Use of Computers in Radiation Therapy*, edited by D. D. Leavitt and G. Starkschall (Medical Physics Publishing, Madison, 1997), pp. 406–409.
[10]A. Ahnesjö, P. Andreo, and A. Brahme, ''Calculation and application of point spread functions for treatment planning with high energy photon beams,'' Acta Oncolog. **26**, 49–56 (1987).
[11]H. A. Bethe and J. Askhin, ''Passage of radiations through matter,'' in *Experimental Nuclear Physics*, Vol. 1, edited by E. Segrè (Wiley, New York, 1953).
[12]J. F. Janni, ''Proton range-energy tables, 1 keV–10 GeV,'' At. Data Nucl. Data Tables **27**, 147–339 (1982).
[13]M. J. Berger, ''Penetration of proton beams through water I. Depth-dose distribution, spectra and LET distribution,'' Report NISTIR 5226, National institute of standards and technology, physics laboratory, Gaithersburg, MD 20899, July 1993.
[14]R. D. Evans, *The Atomic Nucleus* (Robert E. Krieger, Malabar, FL, 1982). Reprint.
[15]M. R. Raju, *Heavy Particle Radiotherapy* (Academic, New York, 1980).
[16]ICRU Report 49: Stopping powers and ranges for protons and alpha particles. International Commission on Radiation Units and Measurements, Bethesda, MD, 1993.
[17]H. Bichsel and T. Hiraoka, ''Energy spectra and depth-dose curves for 70 MeV protons,'' Int. J. Quantum Chem. Quantum Chem. Symp. **23**, 565–574 (1989).
[18]M. Abramowitz and I. A. Stegun, Eds., *Handbook of Mathematical Functions* (Dover, New York, 1972).
[19]I. S. Gradshteyn and I. M. Ryzhik, *Table of Integrals, Series and Products* (Academic, San Diego, 1980). Corrected and enlarged edition.
[20]W. T. Chu, B. A. Luedewigt, and T. R. Renner, ''Instrumentation for treatment of cancer using proton and light-ion beams,'' Rev. Sci. Instrum. **64**, 2055–2122 (1993).
[21]H. Bichsel, ''Calculated Bragg curves for ionization chambers of different shapes,'' Med. Phys. **22**, 1721–1726 (1995).

[22]B. Larsson, ''Pre-therapeutic physical experiments with high energy protons,'' Br. J. Radiol. **34**, 143–151 (1961).
[23]A. M. Koehler, R. J. Schneider, and J. M. Sisterson, ''Range modulators for protons and heavy ions,'' Nucl. Instrum. Methods Phys. Res. **131**, 437–440 (1975).
[24]U. Oelfke, K. -U. Gardey, E. W. Blackmore, and G. K. Y. Lam, ''Proton dosimetry at TRIUMF: Experimental profiles and PTRAN MC calculations,'' in PTCOG XXI, San Francisco, April 25 1995.
[25]R. R. Wilson, ''Range, straggling, and multiple scattering of fast protons,'' Phys. Rev. **71**, 385–386 (1947).